Large-Scale 3D Baseline Measurement Based on Phase-Stabilized GNSS-Over-Fiber System

Xin Jiang, Xiangchuan Wang, Xi Liu, Lugang Wu, Chaosheng Huang, Jianbin Fu, Yu Xiang, Jianping Yao, *Fellow, IEEE, Fellow, OSA*, and Shilong Pan, *Senior Member, IEEE*

***Abstract*—Multi-antenna GNSS-over-fiber system is considered an effective solution for three-dimension (3D) baseline measurement. By precisely determining the transmission time delays between the antennas and the receiver, the vertical precision can be improved based on the single difference (SD) model. This method, however, would encounter problems if the baseline is too long, since a high precision measurement of the time delay of a long fiber link is usually time-consuming. Here, we propose and demonstrate a high-speed phase-stabilized GNSS-over-fiber system for large-scale 3D baseline measurement. A relatively slow but accurate time delay measurement module is used to calibrate the link delay, then a fast active compensation device is employed to keep the time delay constant. If the delay variation exceeds the compensation range, the time delay measurement module would measure the link delay again and bias the active compensation device at a new operating state. In a proof-of-concept experiment, the precision of the 3D baseline measurement obtained by the proposed system with a 20-km optical fiber is around 2.82 mm thanks to the rigid active compensation and the high-precision time delay measurement. If the active compensation device is disabled, the vertical precision of the baseline measurement obtained would be degraded from 2.82 mm to 16.46 mm in 10 minutes.**

***Index Terms*—3D baseline, GNSS-over-fiber, phase-stabilized configuration, single difference model.**

I. Introduction

THE GLOBAL navigation satellite system (GNSS) has been widely adopted for positioning, navigation and timing for civil aviation, shipping, railways, 5G communication networks and other industries [1]–[3]. In order to meet the demand of high precision measurements, such as attitude determination of vehicles [4], [5] and displacement monitoring [6]–[9] of bridges, towers, and dams, GNSS carrier phase measurement can be implemented to estimate the relative position between two antennas, also known as the multi-direction baseline [10]. In order to reduce the complexity and cost, a GNSS-based baseline measurement system using a single receiver with multiple antennas was proposed [11], [12]. With the increase in the baseline length, a double difference (DD) model based GNSS-over-fiber system was proposed to provide a solution to transfer the GNSS signals with ultralow loss, which also takes advantage of the immunity to electromagnetic interference of optical fiber [13], [14].

Regarding the measurement precision, single difference (SD) model can be utilized to reduce the vertical standard deviation by a factor of about three compared to the standard DD model while clock difference error should be eliminated and the transmission time delay between the antennas and the receiver, also called the line bias, must be calibrated to be within mm level [12]. The former condition can be achieved by utilizing a multi-channel receiver with the same common clock reference source [15]. In order to satisfy the second condition, time delay measurement techniques [16], [17] could be utilized to precisely monitor the line bias variation. Several line bias measurement schemes have been proposed in GNSS-over-fiber systems, which can be generally classified into two categories: phase-derived method [18], [19] and frequency-derived method [20].

In order to obtain a large monitoring range, a long optical fiber should be employed, which will introduce large line bias variations and bring new integer ambiguities to the GNSS carrier phase measurement. The line bias measurement methods mentioned above would encounter problems in such application scenarios. The phase-derived method is implemented based on phase detection of a single frequency signal and thus the effective range is limited to the wavelength of the carrier signal [18], [19]. Although sweeping the frequency in a certain range can overcome the integer ambiguity problem and result in a large measurement range [16], the time needed for an effective measurement would cost more than tens of millisecond, in which the drift of the long fiber might exceed the mm level. On the other hand, in the frequency-derived method, there is a tradeoff between the measurement range and measurement precision.

In this paper, to achieve simultaneously long range and high precision 3D baseline measurement, a phase-stabilized

Manuscript received March 25, 2021; revised June 11, 2021 and July 23, 2021; accepted July 27, 2021. Date of publication August 30, 2021; date of current version November 2, 2021. This work was supported in part by the National Natural Science Foundation of China under Grants 62075095 and 11804159, in part by Young Elite Scientists Sponsorship Program by CAST under Grant 2018QNRC001, and in part by the Key Research and Development Program of Jiangsu Province under Grant BE2020030. *(Corresponding authors: Xiangchuan Wang; Shilong Pan.)*

Xin Jiang, Xiangchuan Wang, Xi Liu, Chaosheng Huang, Yu Xiang, and Shilong Pan are with the Key Laboratory of Radar Imaging and Microwave Photonics (Nanjing University of Aeronautics and Astronautics), Ministry of Education, Nanjing University of Aeronautics and Astronautics, Nanjing 210016, China (e-mail: jiangx@nuaa.edu.cn; wangxch@nuaa.edu.cn; liuxi1210@nuaa.edu.cn; chaoshengh@nuaa.edu.cn; yxiang@nuaa.edu.cn; pans@ieee.org).

Lugang Wu and Jianbin Fu are with the Suzhou LiuYaoSi Information Technologies Co., Ltd., Suzhou 215500, China (e-mail: wlg@newkeytech.com; foo@newkeytech.com).

Jianping Yao is with the Microwave Photonics Research Laboratory, School of Electrical Engineering and Computer Science, University of Ottawa, ON K1N 6N5, Canada (e-mail: jpyao@eecs.uottawa.ca).

Color versions of one or more figures in this article are available at https://doi.org/10.1109/JLT.2021.3108566.

Digital Object Identifier 10.1109/JLT.2021.3108566

configuration based GNSS-over-fiber system is proposed. The round-trip delay correction mechanism can eliminate the phase variation within the delay compensation range. In addition, a time delay measurement is applied to calibrate the line bias if the line bias variation exceeds the delay compensation range. The single frequency signal based active correction method is fast but leads to the integer ambiguity problem if the delay variation exceeds the compensation range, while the time delay measurement is relatively slow due to the frequency sweeping but unambiguous. Thus, the advantage of the combination in the proposed configuration is that it can simultaneously keep the line bias stabilized in a short time and calibrate the unambiguous line bias parameter in a long time to achieve high precision, large range, and stable 3D baseline measurement.

This paper is divided into four sections. In Section II, an analytical model of the 3D baseline measurement based on the SD and the DD carrier phase measurement is established, after which the carrier phase observations in the DD model and the SD model are comparatively analyzed. Simulation analysis of the line bias influence on the precision of the baseline measurement is also implemented, and the principle of the proposed phase-stabilized configuration is introduced. In Section III, a 3D baseline measurement is carried out to compare the 3D baseline measurement results with and without the phase-stabilized configuration. In Section IV, concluding remarks and discussions are provided.

II. Principle

A. GNSS-Based 3D Baseline Measurement

The measurement model of the GNSS carrier phase can be expressed as [20], [21]:

$$\lambda\phi_i^k = \rho_i^k - I_i^k + T_i^k + c(\delta t_i - \delta t^k) + LB_i + \lambda N_i^k + e_i^k \tag{1}$$

where λ denotes the wavelength of the GNSS signal, ϕ_i^k represents the measured carrier phase of the signal transfers from the *k*th satellite to the *i*th antenna, ρ_i^k is the true distance between the antenna and the satellite, *I* represents the ionosphere, *T* denotes the tropospheric delay, *c* represents the speed of light in vacuum, δt is the time shift of the clock, LB_i is the line bias between the receiver and the *i*th antenna, N_i^k is the integer ambiguity of the carrier phase, and e_i^k denotes the noise.

The SD model with a common clock reference source can be established by the differentiation of carrier phases come from the *k*th satellite to the *i*th and the *j*th antennas, i.e.,

$$\lambda\Delta\phi_{ij}^k = \mathbf{s}^k\mathbf{b}^T + \Delta LB_{ij} + \lambda\Delta N_{ij}^k + \Delta e_{ij}^k \tag{2}$$

where T represents the transpose symbol, Δ denotes the SD operation, $\boldsymbol{b} = [\,b_{\mathrm{x}}\ b_{\mathrm{y}}\ b_{\mathrm{z}}\,]$ is the 3D baseline, $\boldsymbol{s}^k = [\,s_{\mathrm{x}}^k\ s_{\mathrm{y}}^k\ s_{\mathrm{z}}^k\,]$ represents the normalized line of sight vector between the antennas and the *k*th satellite. The SD model with *n* observed satellites can be expressed as

$$\lambda\begin{bmatrix}\Delta\phi_{ij}^1\\ \Delta\phi_{ij}^2\\ \cdots\\ \Delta\phi_{ij}^n\end{bmatrix}_{n\times1} = \begin{bmatrix}\mathbf{s}^1\\ \mathbf{s}^2\\ \cdots\\ \mathbf{s}^n\end{bmatrix}\mathbf{b}^T + \begin{bmatrix}1\\ 1\\ \cdots\\ 1\end{bmatrix}\Delta LB_{ij} + \lambda\begin{bmatrix}\Delta N_{ij}^1\\ \Delta N_{ij}^2\\ \cdots\\ \Delta N_{ij}^n\end{bmatrix}_{n\times1} + \begin{bmatrix}\Delta e_{ij}^1\\ \Delta e_{ij}^2\\ \cdots\\ \Delta e_{ij}^n\end{bmatrix} \tag{3}$$

The DD model is obtained by making differences between the reference satellite and other satellites based on the SD model:

$$\lambda\nabla\Delta\phi_{ij}^{kr} = (\mathbf{s}^k - \mathbf{s}^r)\mathbf{b}^T + \lambda\nabla\Delta N_{ij}^{kr} + \nabla\Delta e_{ij}^{kr} \tag{4}$$

where $\nabla\Delta$ denotes the DD operation. (4) shows that only the baseline parameter and the integer ambiguity parameter are left after the DD operation. Similar to (3), the DD model with *n* observed satellites can be expressed as

$$\begin{aligned}&\lambda\begin{bmatrix}\nabla\Delta\phi_{ij}^{1r}\\ \nabla\Delta\phi_{ij}^{2r}\\ \cdots\\ \nabla\Delta\phi_{ij}^{nr}\end{bmatrix}_{(n-1)\times1}\\ &= \begin{bmatrix}\mathbf{s}^1 - \mathbf{s}^r\\ \mathbf{s}^2 - \mathbf{s}^r\\ \cdots\\ \mathbf{s}^n - \mathbf{s}^r\end{bmatrix}\mathbf{b}^T + \lambda\begin{bmatrix}\nabla\Delta N_{ij}^{1r}\\ \nabla\Delta N_{ij}^{2r}\\ \cdots\\ \nabla\Delta N_{ij}^{nr}\end{bmatrix}_{(n-1)\times1} + \begin{bmatrix}\nabla\Delta e_{ij}^{1r}\\ \nabla\Delta e_{ij}^{2r}\\ \cdots\\ \nabla\Delta e_{ij}^{nr}\end{bmatrix}_{(n-1)\times1}\end{aligned} \tag{5}$$

In the DD model, the integer ambiguities can be treated as constant once they are fixed as long as the satellites are kept tracking [10]. In the SD model, the existence of the line bias variation could affect the baseline result, and the large line bias variation could even introduce new integer ambiguities into the raw integer ambiguities. Therefore, the main principle of the proposed work is to utilize a phase-stabilized configuration to maintain the line bias constant within limits. Besides, the integer ambiguities can also be calibrated by a time delay measurement in the situation of large line bias variation.

B. Comparative Analysis of Carrier Phase Observations in the SD Model and the DD Model

After giving the carrier phase measurement principle of the baseline measurement, the theoretical precision of the SD and the DD carrier phases is analyzed without the consideration of the influence of the line bias.

For simplicity, the observation matrix $\boldsymbol{\Phi}_\Delta$ of the carrier phases in the SD model is defined,

$$\boldsymbol{\Phi}_\Delta = \begin{bmatrix}\Delta\phi_{ij}^1\\ \Delta\phi_{ij}^2\\ \cdots\\ \Delta\phi_{ij}^n\end{bmatrix}_{n\times1} = \mathbf{G}\begin{bmatrix}\phi_j^1\\ \phi_i^1\\ \phi_j^2\\ \phi_i^2\\ \cdots\\ \phi_j^n\\ \phi_i^n\end{bmatrix}_{2n\times1} \tag{6}$$

where

$$\mathbf{G} = \begin{bmatrix}1 & -1 & 0 & 0 & \cdots & 0 & 0\\ 0 & 0 & 1 & -1 & \cdots & 0 & 0\\ & & & & \cdots & & \\ 0 & 0 & 0 & 0 & \cdots & 1 & -1\end{bmatrix}_{n\times2n} \tag{7}$$

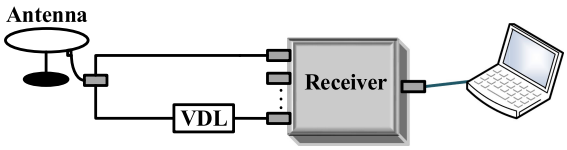

Fig. 1. The zero baseline experiment setup. VDL: variable delay line.

Supposing that the precision of the raw carrier phase (ϕ_j^k) measurement is σ_Φ^2, the variance-covariance matrix of the raw carrier phase measurement can be obtained,

$$\left[\phi_j^1\ \phi_i^1\ \phi_j^2\ \phi_i^2\ \cdots\ \phi_j^n\ \phi_i^n\right]^{\mathrm{T}} \sim \boldsymbol{I}_n\boldsymbol{\sigma}_\phi^2 \tag{8}$$

According to (6), (7), (8) and the variance-covariance propagation law, the variance-covariance matrix Q_{Φ_Δ} of Φ_Δ can be written as

$$\mathbf{Q}_{\mathbf{\Phi}_\Delta} = \mathbf{G}(\mathbf{I}_n\sigma_\phi^2)\mathbf{G}^{\mathrm{T}} = 2\sigma_\phi^2\boldsymbol{I}_n \tag{9}$$

Similarly, the observation matrix $\Phi_{\nabla\Delta}$ in the DD model is defined as

$$\mathbf{\Phi}_{\nabla\Delta} = \begin{bmatrix} \nabla\Delta\phi_{ij}^{\mathrm{m}1} \\ \nabla\Delta\phi_{ij}^{\mathrm{m}2} \\ \nabla\Delta\phi_{ij}^{\mathrm{m}3} \\ \cdots \end{bmatrix}_{(n-1)\times 1} = \mathbf{H}\begin{bmatrix} \Delta\phi_{ij}^{\mathrm{m}} \\ \Delta\phi_{ij}^{1} \\ \Delta\phi_{ij}^{2} \\ \cdots \end{bmatrix}_{n\times 1} \tag{10}$$

where

$$\mathbf{H} = \left[\begin{array}{c|cccc} 1 & -1 & 0 & \cdots & 0 \\ 1 & 0 & -1 & \cdots & 0 \\ 1 & \cdots & \cdots & \cdots & \cdots \\ 1 & 0 & 0 & \cdots & -1 \end{array}\right]_{(n-1)\times n} \tag{11}$$

According to (9), (10), (11) and the variance-covariance propagation law, the variance-covariance matrix $Q_{\Phi_{\nabla\Delta}}$ of $\Phi_{\nabla\Delta}$ can be written as

$$\mathbf{Q}_{\mathbf{\Phi}_{\nabla\Delta}} = \mathbf{H}(2\sigma_\phi^2\mathbf{I}_n)\mathbf{H}^{\mathrm{T}} = 2\sigma_\phi^2\begin{bmatrix} 2 & 1 & \cdots & 1 \\ 1 & 2 & \cdots & 1 \\ \cdots & \cdots & \cdots & \cdots \\ 1 & \cdots & \cdots & 2 \end{bmatrix} \tag{12}$$

Compared (12) with (9), the raw measurement error of the carrier phase σ_ϕ^2 is multiplied by a transfer matrix with larger diagonal elements. Thus, the precision of the carrier phase measurements of the DD model is lower than that of the SD model as long as the line bias maintains constant.

C. The Simulation Analysis of the Line Bias Influence

To investigate the impact of the line bias error on the precision of the baseline measurement, a zero baseline experiment was carried out as shown in Fig. 1 and the fiber used was only about 1 m. There are two significant advantages of the zero baseline experiment. Firstly, the zero baseline is the most ideal reference in theory, thus no other external reference is needed. Secondly, all errors can be eliminated except the line bias error. Thus any departure is an indication of the line bias error and the error of the original carrier phase measurement.

In the simulation, the line bias error was artificially added by a step of 1 mm, the results of the baseline measurement solved by the SD model were recorded. To reduce the influence of satellite constellation distribution, the results were calculated by the same raw observation data under the same distribution situation of satellites. Table I shows the relationship between the line bias error and the baseline error in the SD model. The error propagation coefficients of the three components can be calculated as 0.38, 0.81 and 2.48 separately. It can be concluded that the line bias error has a great influence on the results of the three components of the baseline solved by the SD model, especially in the vertical component.

TABLE I
THE RELATIONSHIP BETWEEN THE LINE BIAS ERROR AND THE BASELINE ERROR IN THE SD MODEL

Line bias error (mm)	East error (mm)	North error (mm)	Vertical error (mm)
1	0.25	0.69	-2.56
2	0.64	1.51	-5.04
3	1.04	2.34	-7.51
4	1.43	3.16	-9.98
5	1.83	3.99	-12.46
6	2.22	4.81	-14.93
7	2.62	5.64	-17.41
8	3.02	6.47	-19.88
9	3.41	7.29	-22.35
10	3.81	8.12	-24.83
11	4.20	8.94	-27.30
12	4.60	9.77	-29.77
13	4.99	10.59	-32.25
14	5.39	11.42	-34.72
15	5.78	12.25	-37.20
16	6.18	13.07	-39.67
17	6.57	13.90	-42.12
18	6.97	14.72	-44.62
19	7.36	15.55	-47.09
20	7.76	16.37	-49.56

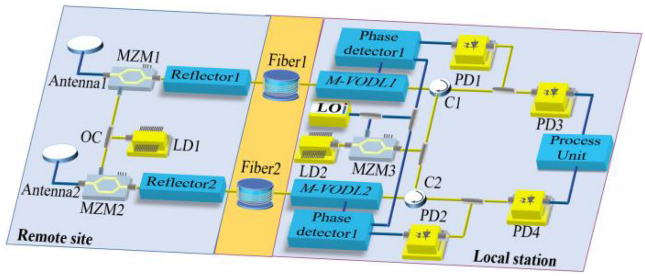

Fig. 2. Schematic diagram of the phase-stabilized configuration based GNSS-over-fiber system. OC: Optical coupler; LD: Laser diode; PD: Photodetector; MZM: Mach-zehnder modulator; C: Circulator; M-VODL: Motorized variable optical delay line.

D. The Principle of the Proposed Phase-Stabilized Configuration

In order to eliminate the huge influence of line bias on the measurement precision, a phase-stabilized configuration is proposed to make the line bias parameter constant in this section.

The schematic diagram of the phase-stabilized configuration based GNSS-over-fiber system is shown in Fig. 2, which

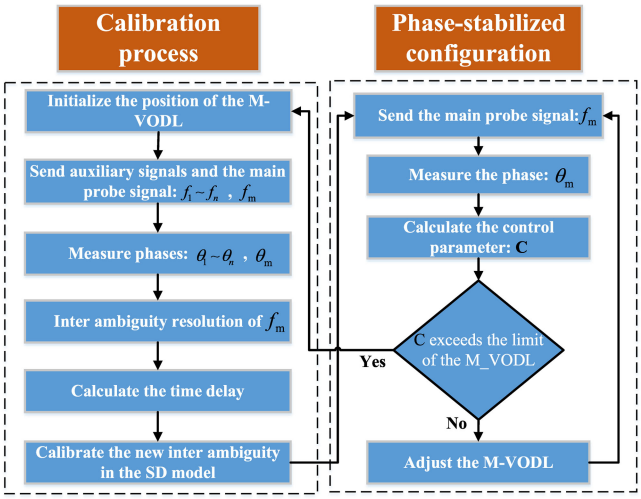

Fig. 3. The control process of the proposed phase-stabilized configuration.

contains multiple GNSS-over-fiber transmission links, phase-stabilized modules, and a multi-channel receiver. At the remote site, GNSS signals are received by the antennas. A lightwave generated by a laser diode (LD) is intensity-modulated by the GNSS signal through a Mach-Zehnder modulator (MZM). As the GNSS signal is very weak, the GNSS signal should be significantly amplified before driving the MZM. A low noise amplifier with large gain and small noise figure can significantly reduce the influence of noise introduced by the GNSS link. The modulated optical signal is transmitted to the local station via an optical fiber and eventually detected by a photodetector (PD).

As shown in Fig. 2, GNSS signals are received by PD3 and PD4. The multi-channel GNSS receiver is responsible for decoding navigation data and measuring the carrier phase.

The control process of the proposed phase-stabilized configuration is shown in Fig. 3. The phase change of the highest frequency signal is continuously measured as the feedback control signal of a motorized variable optical delay line (M-VODL). Thus the line bias can maintain constant within the delay compensation range. The new integer ambiguity calibration of the line bias is based on the time delay measurement in which several other auxiliary signals help to solve the ambiguity of the highest frequency signal. Firstly, the initialization process is performed which consists of M-VODL initialization and time delay measurement. To make full use of the range of the M-VODL, we center the M-VODL in the middle. Then the phase-stabilized module starts to run continuously in which the control parameter is calculated according to the phase change of the highest frequency signal. If the variation of the line bias is beyond the range of the M-VODL, the initialization process will be performed.

The relationship between the time delay and the phase of the highest frequency signal can be written as:

$$\tau = -\frac{\theta_m + 360N_m}{360f_m} \tag{13}$$

Here θ_m and f_m are the phase and the frequency of the highest frequency signal.

In the phase-stabilized process, the control parameter C is calculated to control the time delay of the M-VODL according to the accumulation of the time delay variation and can be expressed as:

$$C(t_n) = \frac{\sum_{i=0}^{n} d\theta_m(t_i)}{360f_m} \tag{14}$$

Here, $d\theta_m$ is the phase change of the highest frequency signal.

To calibrate the new integer ambiguity of the line bias, the time delay value needs to be achieved [22]. Here, we give the principle of the time delay measurement. First, two auxiliary signals f_1 and f_2 with a small frequency interval Δf are chosen to guarantee that their integer ambiguities are equal. So the phases of the two 'relatively unambiguous' signals can be expressed as

$$\begin{cases} \theta_1 = (-f_1\tau - N_1) \times 360 \\ \theta_2 = (-f_2\tau - N_2) \times 360 \end{cases} \tag{15}$$

Here, the integer ambiguities of the two auxiliary signals are equal, $N_1 = N_2$. Thus, an initial delay estimation τ_2 can be obtained as

$$\tau_2 = -\frac{\theta_2 - \theta_1}{(f_2 - f_1) \times 360} \tag{16}$$

Next, τ_i is utilized to solve the relative integer ambiguity N'_{i+1} between the next auxiliary signal f_{i+1} and f_1 by a rounding operation,

$$N'_{i+1} = round[(\theta_1 - k_f \times \tau_i - \theta_{i+1})/360] \tag{17}$$

It should be noted that the choice of the next auxiliary signal is based on a predefined 'extension coefficient k_f', which can be expressed as

$$k_f = \frac{f_{i+1} - f_1}{f_i - f_1} \tag{18}$$

With the known relative integer ambiguity between f_{i+1} and f_1, the next delay estimation τ_{i+1} can be obtained,

$$\tau_{i+1} = -\frac{\theta_{i+1} - \theta_1 + 360N'_{i+1}}{(f_{i+1} - f_1) \times 360} \tag{19}$$

By extending the frequency of the auxiliary signals gradually, we can obtain a delay estimation τ_m with enough precision to determine the ambiguity of the highest frequency signal, which can be expressed as:

$$N_m = round(-\tau_m f_m) \tag{20}$$

Finally, the time delay can be calculated based on the measured phase and the integer ambiguity of the highest frequency via (13).

E. The Flowchart of the 3D Baseline Solution

Fig. 4 gives the flowchart of the 3D baseline solution with the proposed phase-stabilized configuration. The raw observation data of the distributed antenna is transmitted to the receiver via an optical fiber. Then, the receiver outputs the carrier phases, the ephemeris of the satellites, and the rough position of the antenna after decoding the raw observation data. In the data processing center, the SD model is performed with a constant

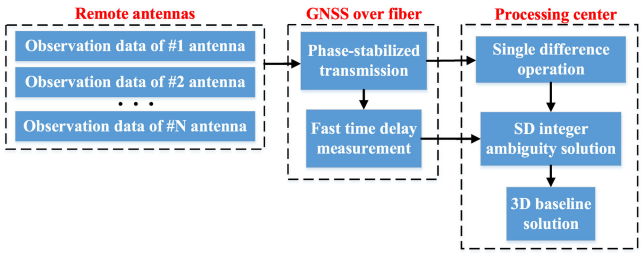

Fig. 4. Flowchart of the 3D baseline solution based on the proposed phase-stabilized configuration.

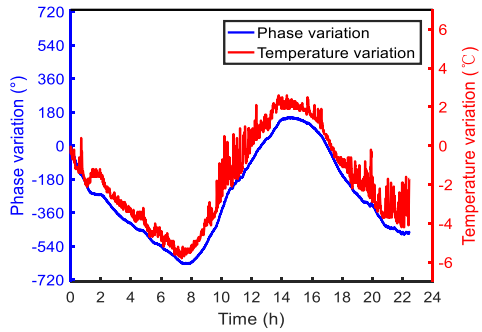

Fig. 5. The phase variation (1575.42 MHz) and temperature variation in one day.

TABLE II
THE RAW AND THE CORRECTED PHASES OF THE FIVE SIGNALS IN THE MEASUREMENT

Frequencies (MHz)	Raw phases (degree)	Corrected phases with relative integer ambiguities (degree)
990	54.87	54.87
990.002	-76.83	-76.83
990.02	78.97	-1361.03
990.2	-132.87	-14172.87
992	-112.61	-142312.61
1000	-106.59	-711826.59

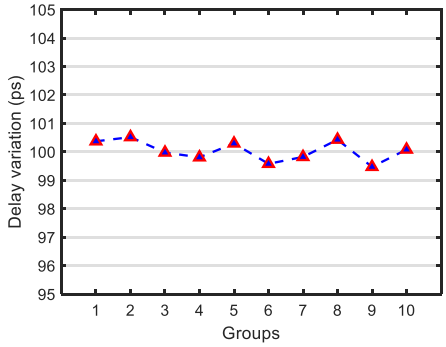

Fig. 6. The calculated delay variations in the time delay measurement.

line bias parameter with the help of the phase-stabilized module as described in Section D. Finally, the 3D baseline can be obtained with fixed integer ambiguities.

III. EXPERIMENT RESULTS AND DISCUSSION

A. The Line Bias Variation in One Day

To investigate the line bias variation in a GNSS-over-fiber link, a single-frequency signal with 1575.42 MHz was utilized to monitor the phase variation. In the experiment, a 2.01-km single-mode fiber was utilized as transmission link under test. Meanwhile, a temperature sensor was put inside the optical fiber disk to monitor the temperature variation.

Fig. 5 shows the phase variation of the 1575.42-MHz signal and temperature change in one day, which leads to the following remarks,

1) There is a high degree of consistency between the phase variation of the transmission signal and temperature variation.
2) The range of the line bias variation reaches 1.6 ns in a 2.01-km single-mode fiber with a temperature change of 8 degrees. Thus, the line bias will increase to several nanoseconds or even tens of nanoseconds with the increase of the fiber length, which would exceed the delay compensation range of an M-VODL.

B. The Performance of the Phase-Stabilized Configuration

First, an experiment was designed to test the performance of the time delay measurement for the line bias calibration.

At the remote site, a 1550-nm laser source (TeraXion) and a 10-GHz MZM (Lucent 2623NA) were used for electrical-to-optical modulation. At the local station, 10-GHz PDs (CONQUER) with a responsivity of 0.65 A/W were utilized for optical-to-electrical conversion. In the phase-stabilized module at the local station, a signal generator (Keysight N5183B MXG) generated the single-tone signals to detect the line bias variation. A phase detector compared the phase difference between the reference and the round-trip signals. An M-VODL with an OEM controller board executed the commands from the control unit and the range of the M-VODL is 560 ps. The length of the transmission optical fiber was about 20 km. The highest frequency was set as 1 GHz. The frequencies of the auxiliary signals were 990 MHz, 990.002 MHz, 990.02 MHz, 990.2 MHz, and 992 MHz, respectively. In the experiment, the M-VODL was utilized to introduce a certain line bias variation within 100 ps. With a precision of 10 fs, the M-VODL can also be used as a delay variation reference. The M-VODL was moved from 0 to 100 ps for 10 times, the raw and the corrected phases of the five signals in the measurement are shown in Table II.

According to the corrected phases of 990 MHz and 1000 MHz, the delay can be calculated with high enough precision to obtain the integer ambiguity of the 1000 MHz signal which is -197745. Thus, the round-trip delay can be obtained as 197745296.09 ps. All the delay variations calculated by the time delay measurement in the 20-km optical fiber are shown in Fig. 6. The standard deviation of the 10 measurements is 0.364 ps which is high enough for the high precision line bias calibration.

Next, a zero baseline configuration similar to Fig. 1 was set up to test the phase-stabilized performance. Similarly, a 20-km optical fiber was introduced as one of the transmission links. The highest frequency of the probe signal was set as 1 GHz. The

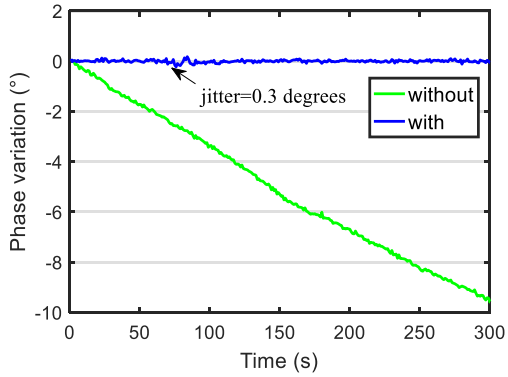

Fig. 7. The phase variation of the highest frequency signal with and without the phase-stabilized configuration.

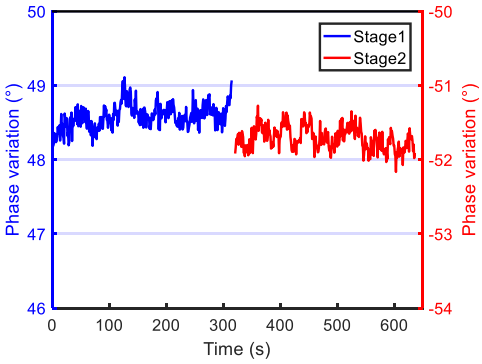

Fig. 8. Phase variation when the delay variation exceeds compensation range.

phase variation of the 1 GHz signal was depicted in Fig. 7. The phase maintained relatively constant and the phase jitter was less than 0.3 degrees with the phase-stabilized configuration. If the phase-stabilized configuration was disabled, the phase drifts significantly.

The experimental result when the link delay variation exceeds the compensation range is presented in Fig. 8. During stage 1, the phase of the 1 GHz signal was stabilized at about 48.20 degrees and the delay calibration result was 98069866.12 ps. When the delay variation exceeded the compensation range, the delay calibration was carried out and the result was 98070144.21 ps, then the phase of the 1 GHz signal was restabilized at about -51.92 degrees. The recalibration process consists of the reset of the compensation device and the time delay measurement. During the recalibration, the high precision baseline measurement by the SD solution cannot be realized. Thus, the baseline measurement obtained by the DD solution is recommended to replace that obtained by the SD solution.

C. The SD and DD Carrier Phase Measurements in a Zero Baseline Experiment

To investigate the impact of the line bias variation on the SD and DD carrier phase measurements, zero baseline experiments were carried out with and without the phase-stabilized configuration, as shown in Fig. 9 and Fig. 10. It can be observed that the vibrations introduced by the line bias directly affected all the SD carrier phase measurements in Fig. 9(b). Nevertheless, the

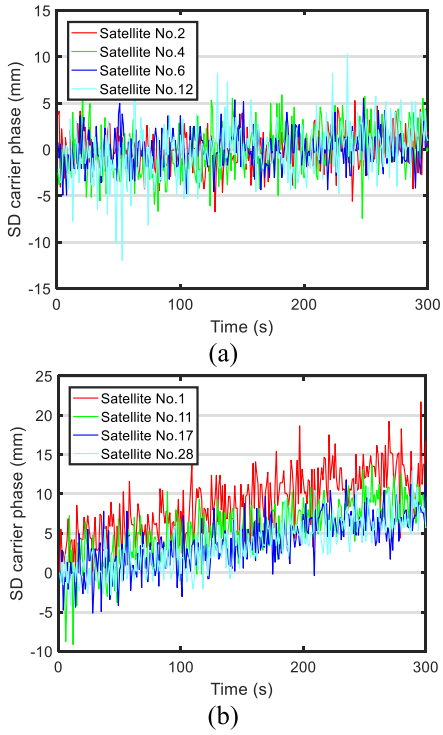

Fig. 9. The SD carrier phase measurements (a) with and (b) without the phase-stabilized configuration.

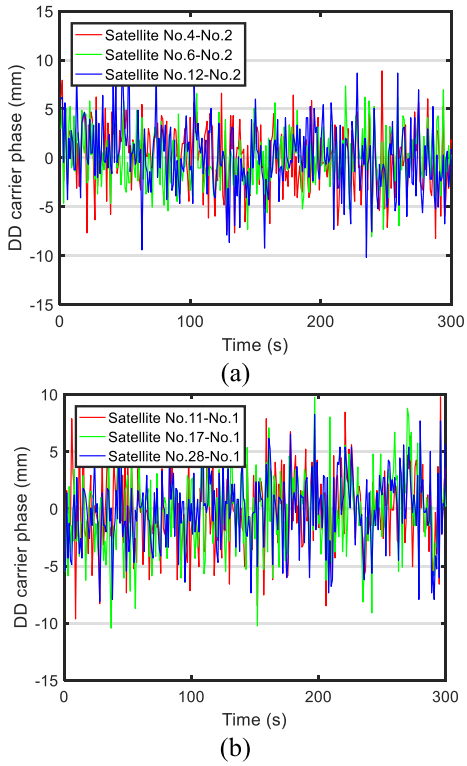

Fig. 10. The DD carrier phase measurements with (a) and without (b) the phase-stabilized configuration.

TABLE III
THE STANDARD DEVIATIONS OF THE SD CARRIER PHASE MEASUREMENTS WITH THE PHASE-STABILIZED CONFIGURATION IN THE ZERO BASELINE EXPERIMENT

Satellite number	Standard deviations
No.2	1.95 mm
No.4	2.66 mm
No.6	1.97 mm
No.12	2.91 mm

TABLE IV
THE STANDARD DEVIATIONS OF THE SD CARRIER PHASE MEASUREMENTS WITHOUT THE PHASE-STABILIZED CONFIGURATION IN THE ZERO BASELINE EXPERIMENT

Satellite number	Standard deviations
No.1	4.48 mm
No.11	4.02 mm
No.17	3.69 mm
No.28	3.82 mm

TABLE V
THE STANDARD DEVIATIONS OF THE DD CARRIER PHASE MEASUREMENTS WITH THE PHASE-STABILIZED CONFIGURATION IN THE ZERO BASELINE EXPERIMENT

Satellite number	Standard deviations
No.4-No.2	3.26 mm
No.6-No.2	2.83 mm
No.12-No.2	3.45 mm

TABLE VI
THE STANDARD DEVIATIONS OF THE DD CARRIER PHASE MEASUREMENTS WITHOUT THE PHASE-STABILIZED CONFIGURATION IN THE ZERO BASELINE EXPERIMENT

Satellite number	Standard deviations
No.11-No.1	3.41 mm
No.17-No.1	3.40 mm
No.28-No.1	3.18 mm

DD carrier phase measurements were not disturbed by the line bias variation as shown in Fig. 10.

Table III, Table IV, Table V and Table VI are the statistical results of the SD and the DD carrier phase measurements in the zero baseline experiment. On the one hand, the mean standard deviation of the SD and the DD carrier phase measurements are 2.37 mm and 3.18 mm with the phase-stabilized configuration. Thus, the precision of the SD carrier phase measurements is more precise than that of the DD carrier phase measurements. Meanwhile, the statistical results agree well with the prediction of (9) and (12). On the other hand, the standard deviations of the DD carrier phase measurements are almost the same in both cases which are 3.18 mm and 3.33 mm, respectively. Therefore, our analysis shows that the SD model outperforms the DD model only when the line bias variation is obtained or eliminated precisely.

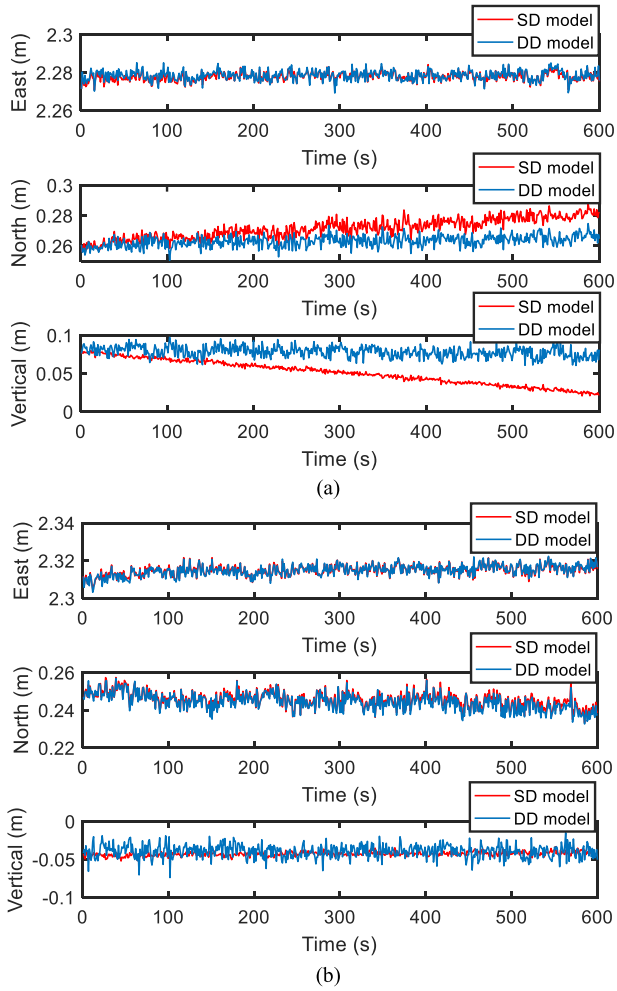

Fig. 11. Baseline measurement results using the conventional DD model and the SD model (a) without and (b) with the phase-stabilized configuration.

D. The Performance of the Proposed GNSS-Based 3D Baseline Measurement System

In the experiment, remote GNSS antennas were fixedly installed on the roof of a building. To emulate the practical large-scale measurement application, a 20-km optical fiber was utilized to connect one of the remote GNSS antennas and the local receiver. The phase-stabilized module and other processing units including a multi-channel GNSS receiver and a computer were placed indoors.

Two groups of experiments were conducted to investigate the performance of the proposed system by comparing the 3D baseline results of the conventional DD model and the SD model. Fig. 11(a) shows the baseline measurement results without the phase-stabilized configuration. The east component of the baseline measurement results achieved by the SD model and the DD model is very close, which means the line bias variation has little effect on the east component which is due to the good symmetry of the satellites in the east-west direction. The north component of the baseline measurement results achieved by the SD model shows an obvious drift compared with that of the DD model. That means the symmetry of the satellites is poorer in

TABLE VII
THE STANDARD DEVIATIONS OF THE 3D BASELINE MEASURED BY THE CONVENTIONAL DD MODEL AND THE SD MODEL WITH AND WITHOUT THE PHASE-STABILIZED CONFIGURATION

3D baseline	DD (without)	SD (without)	DD (with)	SD (with)
East (mm)	2.58	2.20	3.01	2.82
North (mm)	3.63	6.61	4.58	4.30
Vertical (mm)	7.29	16.46	8.61	2.82

the north-south direction. In the vertical direction, because the vertical distribution of the satellites is completely asymmetric, a more obvious drift can be observed. The standard deviation increases to 16.46 mm as shown in Table VII, which is much worse than that of the DD model.

Fig. 11(b) shows the baseline measurement results with the phase-stabilized configuration. The east and the north components of the baseline measurement results obtained by the SD model and the DD model are very close. From the statistical results in Table VII, it can be found that the horizontal precision of the baseline obtained by the SD model is slightly better than that of the DD model. Regarding the vertical component of the baseline, the standard deviations obtained by the DD model and the SD model are 8.61 mm and 2.82 mm separately, indicating an improvement of 205%.

These experimental results show that the baseline measurement results of the DD model are independent of the line bias variation, but the precision of the vertical component is always 2-3 times poorer than those of the horizontal components. The baseline measurement results of the SD model are strongly affected by the line bias variation. Under the circumstance without compensation, the line bias variation will transfer to the three components of the baseline measurement according to the distribution of satellites in the SD model.

IV. CONCLUSION

A multi-antenna GNSS-over-fiber system with a phase-stabilized configuration was proposed for large-scale 3D baseline measurement. By utilizing the phase-stabilized configuration, the 3D baseline measurement obtained by the SD model enables highly precise results in all three directions. In addition, a time delay method is proposed to calibrate the unambiguous line bias parameter both in the initial stage and in the case when the line bias variation exceeds the delay compensation range. In the proof-of-concept experiment, the phase jitter of the monitoring signal was less than 0.3 degrees and the line bias calibration precision reached 0.364 ps. The 3D baseline measurement results showed that the SD model outperformed the DD model with the assistance of the phase-stabilized configuration.

REFERENCES

[1] L. Yin, Q. Ni, and Z. Deng, "A GNSS/5G integrated positioning methodology in D2D communication networks," *IEEE J. Sel. Areas Commun.*, vol. 36, no. 2, pp. 351–362, Feb. 2018.
[2] D. Peng, E. M. Hill, L. Li, A. D. Switzer, and K. M. Larson, "Application of GNSS interferometric reflectometry for detecting storm surges," *GPS Solut.*, vol. 23, no. 2, pp. 1–11, 2019.
[3] N. Z. Wang, T. H. Xu, F. Gao, and G. C. Xu, "Sea level estimation based on GNSS dual-frequency carrier phase linear combinations and SNR," *Remote Sens*, vol. 10, no. 3, 2018, Art. no. 470.
[4] T. Xu, L. Xu, X. Tian, and X. Li, "GPS-aided method for platform attitude determination based on target images," *Appl. Opt.*, vol. 56, no. 8, pp. 2378–2387, 2017.
[5] A. R. Vetrella, F. Causa, A. Renga, G. Fasano, D. Accardo, and M. Grassi, "Multi-UAV carrier phase differential GPS and vision-based sensing for high accuracy attitude estimation," *J. Intell. Robot. Syst.*, vol. 93, no. 1/2, pp. 245–260, 2018.
[6] H. Wang, P. Xiang, and L. Jiang, "Optical fiber sensor based in-field structural performance monitoring of multilayered asphalt pavement," *J. Lightw. Technol.*, vol. 36, no. 17, pp. 3624–3632, Sep. 2018.
[7] K. Chen, M. Guo, Y. Yang, K. Liu, W. Cai, and Q. Yu, "A fiber-optic displacement sensor based on high-precision differential phase measurement," *IEEE J. Lightw. Technol.*, vol. 36, no. 18, pp. 4046–4050, Sep. 2018.
[8] Y. Yang, D. Tian, K. Chen, X. Zhou, Z. Gong, and Q. Yu, "A fiber-optic displacement sensor using the spectral demodulation method," *IEEE J. Lightw. Technol.*, vol. 36, no. 17, pp. 3666–3671, Sep. 2018.
[9] Y. Tanaka, M. Nemoto, and Y. Yamada, "Displacement measurement using two-photon absorption process in Si-avalanche photodiode and fiber bragg gratings," *J. Lightw. Technol.*, vol. 36, no. 4, pp. 1192–1196, Feb. 2018.
[10] G. Xie, *Principles of GPS and Receiver Design*. Beijing, China: Publishing House of Electronics Industry, 2009.
[11] Y. Q. Chen, X. L. Ding, D. F. Huang, and J. J. Zhu, "A multi-antenna GPS system for local area deformation monitoring," *Earth Planets Space*, vol. 52, no. 10, pp. 873–876, 2000.
[12] R. Santerre and G. Beutler, "A proposed GPS method with multi-antennae and single receiver," *Bull. Géodésique*, vol. 67, no. 4, pp. 210–223, 1993.
[13] L. M. Pessoa, J. M. B. Oliveira, D. Coelho, J. C. S. Castro, H. M. Salgado, and M. Fames, "Transmission of differential GPS signals over fiber for aircraft attitude determination," in *Proc. IEEE Avionics, Fiber-Opt. Photon. Dig. CD*, 2012, pp. 80–81.
[14] J. M. B. Oliveira, L. M. Pessoa, H. M. Salgado, G. Proudley, D. Charlton, and H. White, "Experimental evaluation of a differential GPS-over-fiber system for aircraft attitude determination," in *Proc. IEEE Avionics, Fiber-Opt. Photon. Technol. Conf.*, 2013, pp. 75–76.
[15] J. Keong, "GPS/GLONASS attitude determination with a common clock using a single difference approach," in *Proc. 12th Int. Tech. Meet. Satell. Division Inst. Navig.*, Nashville, TN, 1999, pp. 1941–1950.
[16] X. C. Wang *et al.*, "High accuracy optical time delay measurement in fiber link," *Chin. Opt. Lett.*, vol. 17, no. 6, 2019, Art. no. 060601.
[17] S. Li, T. Qing, J. Fu, X. Wang, and S. Pan, "High-accuracy optical fiber transfer delay measurement using fiber-optic microwave interferometry," *IEEE J. Lightw. Technol.*, vol. 39, no. 2, pp. 627–632, Jan. 2020.
[18] D. Macias-Valadez, R. Santerre, S. Larochelle, and R. Landry, "Improving vertical GPS precision with a GPS-over-fiber architecture and real-time relative delay calibration," *GPS Solut.*, vol. 16, no. 4, pp. 449–462, 2011.
[19] X. C. Wang, X. Jiang, S. P. Li, and S. L. Pan, "Multiantenna GPS-over-fiber system for attitude determination using phase-derived range measurement," *IEEE Photon. J.*, vol. 11, no. 4, Aug. 2019, Art. no. 5501610.
[20] X. Jiang, X. C. Wang, A. R. Zhao, J. P. Yao, and S. L. Pan, "A multi-antenna GNSS-over-fiber system for high accuracy three-dimensional baseline measurement," *J. Lightw. Technol.*, vol. 37, no. 17, pp. 4201–4209, Sep. 2019.
[21] Y. Dong, L. Zhang, D. Wang, Q. Li, J. Wu, and M. Wu, "Low-latency, high-rate, high-precision relative positioning with moving base in real time," *GPS Solut.*, vol. 24, no. 2, 2020, Art. no. 56.
[22] S. Li, T. Qing, J. Fu, X. Wang, and S. Pan, "High-accuracy and fast measurement of optical transfer delay," *IEEE Trans. Instrum. Meas.*, vol. 70, pp. 1–4, 2021.

Xin Jiang received the B.S. degree in information engineering from the Nanjing University of Aeronautics and Astronautics, Nanjing, China, in 2014, the B.S. degree in radioengineering from the National University of Aeronautics and Astronautics of Zukovsky, Kharkov, Ukraine, in 2014, and the M.S. degree in 2017 in navigation guidance and control from the Nanjing University of Aeronautics and Astronautics, Nanjing, China, where he is currently working toward the Ph.D. degree in communication and information system. His research interests include GNSS application in engineering, photonic microwave measurement, and photonic technologies for signal processing.

Xiangchuan Wang received the B.Eng. degree in automation and the Ph.D. degree in microelectronics and solid-state electronics from Nanjing University, Nanjing, China, in 2009 and 2015, respectively. He is currently an Associate Professor with the Key Laboratory of Radar Imaging and Microwave Photonics, Ministry of Education, Nanjing University of Aeronautics and Astronautics, Nanjing, China. His current research interests include microwave photonic measurement and optical fiber sensing technologies.

Xi Liu received the B.S. degree from the Nanjing University of Aeronautics and Astronautics, Nanjing, China, in 2019. He is currently working toward the M.S. degree with the Key Laboratory of Radar Imaging and Microwave Photonics, Ministry of Education, Nanjing University of Aeronautics and Astronautics, Nanjing, China. His research focuses on microwave photonics measurement.

Lugang Wu received the M.S. degree from the Nanjing University of Aeronautics and Astronautics, Nanjing, China, in 2017. He is currently with the Suzhou LiuYaoSi Information Technologies Co., Ltd, Suzhou, China. His research include microwave photonics measurement.

Chaosheng Huang received the B.S. degree from the Shanghai Jiao Tong University, Shanghai, China, in 2020. He is currently working toward the M.S. degree with the Key Laboratory of Radar Imaging and Microwave Photonics, Ministry of Education, Nanjing University of Aeronautics and Astronautics, Nanjing, China. His research focuses on microwave photonics measurement.

Jianbin Fu received the B.S. degree in electronic information science and technology, and the Ph.D. degree in communication and information system from the Nanjing University of Aeronautics and Astronautics, Nanjing, China, in 2011 and 2021, respectively. He is currently with the Newkey Photonics Technologies (Suzhou LiuYaoSi Information Technologies Co., Ltd., Suzhou, China). His research interests include microwave photonics, signal processing, distributed radar systems, and optoelectronic measurement.

Yu Xiang received the B.S. degree in optical engineering from Zhejiang University, Hangzhou, China, in 2006, and the M.S. degree in photonics from the Royal Institute of Technology (KTH), Stockholm, Sweden, in 2008, and the Ph.D. degree in applied physics from KTH in 2014, working on design and fabrication of GaAs-based vertical-cavity surface-emitting transistor-lasers. In 2015, he joined the Key Laboratory of Radar Imaging and Microwave Photonics (Nanjing Univ. Aeronaut. Astronaut.), Ministry of Education. He is currently a Lecturer of electronic and information engineering with research focuses on the development of GaAs-based integrated optoelectronic devices and circuits for microwave photonics applications.

Jianping Yao (Fellow, IEEE) received the Ph.D. degree in electrical engineering from the Universite de Toulon, Toulon, France, in December 1997.

He is currently a Professor and the University Research Chair of the School of Electrical Engineering and Computer Science, University of Ottawa, Ottawa, ON, Canada. In 1998, he joined the School of Electrical and Electronic Engineering, Nanyang Technological University, Singapore, as an Assistant Professor. In December 2001, he joined as an Assistant Professor the School of Electrical Engineering and Computer Science, University of Ottawa, where he became an Associate Professor in 2003, and a Full Professor in 2006. In 2007, he was appointed the University Research Chair of microwave photonics. From July 2007 to June 2010, he was the Director of the Ottawa-Carleton Institute for Electrical and Computer Engineering. In 2013, he was reappointed as the Director of the Ottawa-Carleton Institute for Electrical and Computer Engineering. He has authored or coauthored more than 500 papers, including more than 290 papers in peer-reviewed journals and 210 papers in conference proceedings. He was the Guest Editor of the Focus Issue on Microwave Photonics in Optics Express in 2013 and a Feature Issue on Microwave Photonics in Photonics Research in 2014. He is currently the Topical Editor of the *Optics Letters*, and is on the Editorial Board of the IEEE TRANSACTIONS ON MICROWAVE THEORY AND TECHNIQUES, and *China Science Bulletin*.

He is the Chair of numerous international conferences, symposia, and workshops, including the Vice Technical Program Committee (TPC) Chair of the IEEE Microwave Photonics Conference in 2007, the TPC Cochair of the Asia-Pacific Microwave Photonics Conference in 2009 and 2010, the TPC Chair of the high-speed and broadband wireless technologies subcommittee of the IEEE Radio Wireless Symposium in 2009–2012, the TPC Chair of the microwave photonics subcommittee of the IEEE Photonics Society Annual Meeting in 2009, the TPC Chair of the IEEE Microwave Photonics Conference in 2010, the General Cochair of the IEEE Microwave Photonics Conference in 2011, the TPC Cochair of the IEEE Microwave Photonics Conference in 2014, and the General Cochair of the IEEE Microwave Photonics Conference in 2015. He was the recipient of the 2005 International Creative Research Award at the University of Ottawa, the 2007 George S. Glinski Award for Excellence in Research, and the OSA Outstanding Reviewer Award in 2012. From 2013 to 2015, he was an IEEE MTT-S Distinguished Microwave Lecturer. He is a registered Professional Engineer of Ontario. He is a Fellow of the Optical Society of America and the Canadian Academy of Engineering.

Shilong Pan (Senior Member, IEEE) received the B.S. and Ph.D. degrees in electronics engineering from Tsinghua University, Beijing, China, in 2004 and 2008, respectively. From 2008 to 2010, he was a "Vision 2010" Postdoctoral Research Fellow with the Microwave Photonics Research Laboratory, University of Ottawa, Ottawa, ON, Canada. In 2010, he joined the College of Electronic and Information Engineering, Nanjing University of Aeronautics and Astronautics, Nanjing, China, where he is currently a Full Professor and the Executive Director with the Key Laboratory of Radar Imaging and Microwave Photonics, Ministry of Education. He has authored or coauthored more than 340 research papers, including more than 180 papers in peer-reviewed journals and 160 papers in conference proceedings. His research focuses on microwave photonics, which include optical generation and processing of microwave signals, analog photonic links, photonic microwave measurement, and integrated microwave photonics. He is currently a Topical Editor of the *Chinese Optics Letters*. He was the recipient of an OSA Outstanding Reviewer Award in 2015 and a Top Reviewer for the *Journal of Lightwave Technology* in 2016. He is the Chair of numerous international conferences and workshops, including the TPC Chair of the International Conference on Optical Communications and Networks in 2015, the TPC Co-Chair for the IEEE International Topical Meeting on Microwave Photonics in 2017, the TPC Chair of the high-speed and broadband wireless technologies subcommittee of the IEEE Radio Wireless Symposium in 2013, 2014, and 2016, the TPC Chair of the Optical fiber sensors and microwave photonics subcommittee of the OptoElectronics and Communication Conference in 2015, and the Chair of the microwave photonics for broadband measurement workshop of International Microwave Symposium in 2015.